Sigma J Eng Nat Sci, Vol. 43, No. 3, pp. 878–886, June, 2025

Sigma Journal of Engineering and Natural Sciences
Web page info: https://sigma.yildiz.edu.tr
DOI: 10.14744/sigma.2025.00076

Research Article

High gain, low-profile, wideband archimedean spiral antenna with hexagonal fractal reflector surface

Rabia Nur SAĞ[1,*], Tolgahan TÜYLÜ[2], Alper ÇALIŞKAN[3], Nurhan TÜRKER TOKAN[3]

[1]*Baykar Technology, Ozdemir Bayraktar National Technology Center, Istanbul, 34488, Türkiye*
[2]*Tusas Turkish Aerospace Industry, Ankara, 06980, Türkiye*
[3]*Department of Electronics and Communication Engineering, Yildiz Technical University, Istanbul, 34220, Türkiye*

ARTICLE INFO

Article history
Received: 16 February 2024
Revised: 26 April 2024
Accepted: 28 May

Keywords:
Archimedean Spiral; Axial Ratio; Balun; Hexagonal Fractal; Wideband

ABSTRACT

A tapered two-arm Archimedean spiral antenna with microstrip balun and fractal-based reflector surface is designed and manufactured. The operating impedance bandwidth of 1:13.3, and 3-dB AR bandwidth of 1:7 fulfills the requirement of high data rate, wideband and wide coverage zone. The antenna and balun are designed on FR-4 dielectric material with 1.6 mm thickness. The termination of the spiral arm is tapered to reduce the antenna size. To achieve a unidirectional radiation pattern, a reflector surface is used. The reflector surface is designed in a hexagonal fractal form in order to enhance the axial ratio and increase the antenna's gain. The radius and height of the reflector backed spiral antenna is 0.174 and 0.135 wavelengths at 150 MHz, respectively.

Cite this article as: Sağ RN, Tüylü T, Çalışkan A, Türker Tokan N. High gain, low-profile, wideband archimedean spiral antenna with hexagonal fractal reflector surface. Sigma J Eng Nat Sci 2025;43(3):878–886.

INTRODUCTION

Wireless communication systems and their components have been developed to meet the fundamental performance requirements such as low latency, high speed, and large data rates. Many conceptual designs have been introduced in the last decade to fulfill the capacity requirements of today's wireless technology. Due to its frequency independent, circularly polarized characteristics, spiral antenna is a good candidate for communication links. There are various types of planar spiral antennas, including Archimedean spiral, equiangular spiral, and rectangular spiral. The operation principle and radiation properties of Archimedean circular and rectangular spiral antennas are given in [1]. The rectangular spiral antenna, which is favored for its broad-band operation and ease of construction is analyzed in [2] using the method of moments. A new rectangular spiral nano-antenna for solar energy harvesting is investigated and analyzed employing the finite integration method in [3]. Using Rumsey's principle, an Archimedean spiral antenna with circular polarization has been developed [4]. Over a broad bandwidth, this antenna's polarization, radiation pattern, and impedance matching remain unchanged. Archimedean and equiangular spiral antennas are designed and analyzed in [5] with and without a ground plane. An

***Corresponding author.**
*E-mail address: nur.sag@std.yildiz.edu.tr

This paper was recommended for publication in revised form by Editor-in-Chief Ahmet Selim Dalkilic

Published by Yıldız Technical University Press, İstanbul, Turkey

ultra-wideband spiral antenna with a cavity backing is proposed in [6]. It utilizes an equiangular spiral surrounded by an Archimedean spiral and is fed by a tapered microstrip balun. A center-raised, cylindrical, absorber-free cavity backs the spiral to minimize backward radiation without reducing efficiency.

Among its many advantages, Archimedean spiral antennas have two major drawbacks. First and foremost, their input impedance is calculated as 188 Ω by Babinet's theorem. A balun is used to convert the 50 Ω coaxial line impedance to the impedance of the spiral antenna. Connecting the radiating spiral arms to a broadband balun that converts the unbalanced coaxial mode into a balanced two-wire transmission line mode is necessary to accomplish the impedance matching characteristic over a wide range of frequencies. Two-arm planar Archimedean spiral antenna fed by a wideband balun with an exponentially tapering ground is presented in [7]. Broadband matching properties for a spiral antenna designed with a Vivaldi-shaped balun is described in [8]. The suggested antenna uses a balun with a Vivaldi form, which is well-known for its broadband capabilities even at a small size, to accomplish the minimal design complexity without inserting the additional construction. In [9], an Archimedean spiral antenna fed by 186 Ω Phelan balun for use in direction finding and radar warning receivers is described. A flexible, side-fed, ultra-wideband spiral antenna with a microstrip tapered infinite balun feed is introduced in [10]. Due to the side-feed, the antenna could be utilized in wearable applications, as compared to the obstructive perpendicular balun feed. The second drawback of spiral antennas is that, since the diameter of the spiral antenna is determined by the wavelength at the lowest operating frequency, the antenna is too large to meet the size demand when low working frequency is required. Many efforts have been made in recent years to minimize the antenna size [11-15]. Around the spiral antenna, a ring that shares the same center as the spiral elements and forms a capacitive cavity, was added to minimize the antenna size [11]. Compared to typical Archimedean spiral antennas operating at the same lowest frequency, the suggested antenna is more than 30% smaller. The planar spiral antenna is miniaturized using the meander line approach described in [12]. The meander line begins at the end of the spiral arms and is rotated with varying amplitudes along the spiral. The combination of a circular ring and tapered arms for miniaturization has been presented [13]. Compared to a standard spiral antenna, the size reduction ratio has been increased up to 15%. Dual-arm wideband spiral antenna with chip resistors placed regularly in the dielectric substrate is given in [14]. The chip resistors are selected to be purely resistive, and attempts have been made to establish their position and number. For the design of a planar spiral antenna, an arm configuration with three sections is proposed in [15]. The design of all three sections is a combination of logarithmic, rooted, and sine equations. The low cut-off frequency of the suggested antenna is 30.2% lower than that of the spiral antenna with the traditional Equiangular spiral arm.

The majority of the spiral antenna designs include cavity-backed structures to ensure unidirectional radiation. The cavity-backed structure increases the spiral antenna's size, weight, and cost. Therefore, it is extremely important to find techniques to reduce the size of low-cost, cavity-backed spiral antennas while improving the gain and axial ratio values. A spiral antenna design for use in positioning and short-range sensing systems is presented in [16]. The antenna has an equiangular spiral shape, and to reduce its size, a meander line is applied. A semi-fractal reflector with a circular unit element is utilized in place of a cavity-backed structure. The antenna works in the frequency range 0.8 - 4.37 GHz which corresponds to 1:5.46 bandwidth, and it has AR bandwidth from 0.9 GHz to 4.37 GHz.

In this work, a two-arm Archimedean spiral antenna operating at low frequencies (starting from 150 MHz) with high gain and low axial ratio is designed. The end of the spiral arm is tapered to reduce antenna size, resulting in a 21.32% reduction in antenna physical area. By using the tapered arm method instead of meander line technique having sine structure with changing amplitudes and frequencies, straightforward production is achieved. To assure unidirectional radiation from the spiral antenna, to achieve circular polarization across a broad frequency range, and to maximize the gain, a fractal reflector surface with a hexagonal pattern has been chosen as the reflector element. The structure of the hexagonal fractal consists of three repetitions. Based on the measurement results, the antenna gain is greater than 5 dBi in the frequency range of 140-930 MHz, excluding the band at 490-630 MHz. Due to the fractal reflector, up to 10 dBi measured gain is achieved. In addition to these benefits of the fractal reflector, the size, weight, and cost of the spiral antenna are lowered.

This article is organized as follows: In the next section, size reduced Archimedean spiral antenna, microstrip balun and fractal-based ground plane are described with basic design theory. In section 3, fabrication details, radiation patterns, the gain, axial ratio and reflection coefficient variations of the design are given. Conclusions are presented in the final section.

STRUCTURE OF THE SPIRAL ANTENNA

Size Reduced Antenna Design

The presented Archimedean spiral antenna is designed for operation between 150 MHz and 1050 MHz. The parameters of a spiral antenna are displayed in Figure 1. In the design of the spiral antenna, the conductor arm width (w), the conductor arm spacing (s), the inner radius (r_2), the outer radius (r_1), and the number of turns (n) are crucial parameters. The two-arm spiral shape is constructed using the design principles outlined in [16].

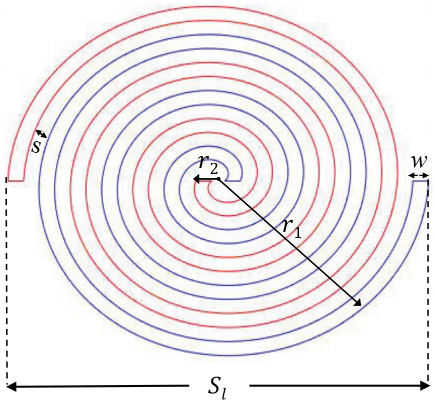

Figure 1. The parameters of a two-arm Archimedean spiral antenna.

The relationship between high-low frequency and inner-outer radius of the spiral antenna is given by Eq. (1) where c is the speed of light. Since the lowest operating frequency of the antenna is 150 MHz, the outer radius is calculated to be 0.3162 m. At 1050 MHz, the inner radius of the antennas is calculated as 0.0454 meters. General design rules for the design of two-arm Archimedean spiral antenna are given in Eq. (1)-(7) [17]. The spiral form of the antenna can be written in cylindrical form as given in Eq. (2).

$$f_{high,low} = c/(2\pi r_{2,1}) \tag{1}$$

$$r_1 = r_0 e^{a\varphi} + r_2 \tag{2}$$

where a refers to angular expansion and $r_0 = (w+s)/\pi$. The width of the conductor arms is calculated with

$$w = (r_1 - r_2)/(2n) - s \tag{3}$$

Finally, the angular growth rate, a and the rotation angle, φ is calculated by Eq. (4-5).

$$a = (2 * w)/\pi \tag{4}$$

$$\varphi = (r_1 - r_2)/a \tag{5}$$

The formulations can be converted to Cartesian coordinates with the following equations:

$$x = (r_2 + a\,\varphi)(cos\,\varphi) \tag{6}$$

$$y = (r_2 + a\,\varphi)(sin\,\varphi) \tag{7}$$

The calculated design parameters of the proposed spiral antenna are listed in Table 1. In radar applications such as subsurface sensing radars and tracking radars, the spiral antenna is commonly employed. As shown in Eq. (1), the physical size of a spiral antenna is determined by its lowest operating frequency. Thus, the spiral antenna becomes very large for practical radar applications.

By using size reduction techniques, the physical area of the spiral antenna may be lowered. Although smaller size is preferred especially for the antennas operating at

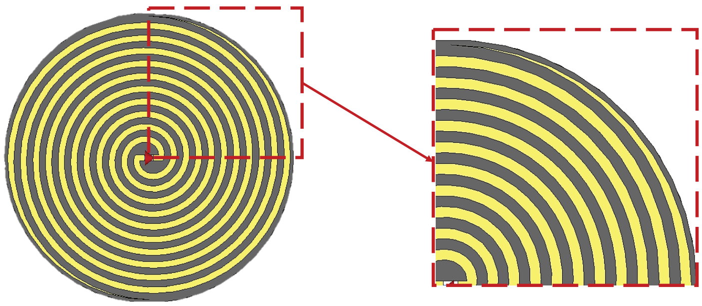

(a)

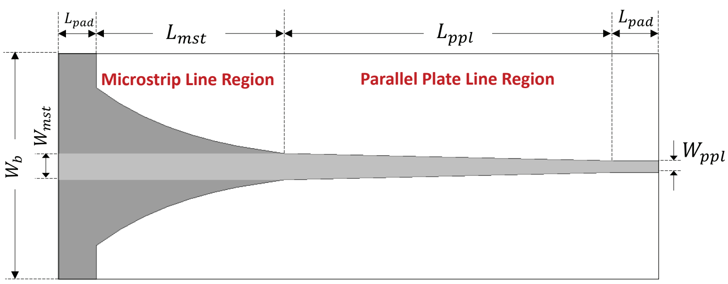

(b)

Figure 2. Tapered arm of the spiral antenna and balun geometry for wide band impedance matching in (a) and (b).

Table 1. Dimensions of the spiral antenna. All units are in mm

Parameter	Value [mm]
S_l	696.2
F_l	710
a	10.504
r_1	348.1
r_2	45
n	5

Table 2. Dimensions of the spiral antenna. All units are in mm

Parameter	Value [mm]
W_b	30
L_{pad}	270
L_{mst}	115
L_{ppl}	145
W_{mst}	3.1
W_{ppl}	0.377

frequencies below microwave frequency band, reduced size may deteriorate the antenna performance and efficiency. Therefore, an optimum point needs to be identified. In this work, the taper line technique is applied to the ends of the spiral arms to reduce the size of the spiral antenna. The common goal of this technique is to minimize the back reflection at the end of the spiral arms and to decelerate the traveling wave. The tapered arm of the spiral antenna is exhibited in the expanded view of spiral antenna given in Figure 2 (a) With the use of tapered arm technique, 21.32% size reduction has been achieved in antenna physical area.

Balun Design

The input impedance of the spiral antenna is theoretically calculated as 188.5 Ω by using Babinet's principle [18]:

$$Z_{in} = \frac{\eta_o}{2} = 188.5\ \Omega \tag{8}$$

Since 50 Ω is used as the system impedance, an impedance matching is required. Balanced and unbalanced feeding, namely balun feeding is suitable for this structure. The FR-4 substrate is used for the 50-188 Ω impedance converter, as well. Figure 2 (b) depicts the geometry of the 50 Ω to 188 Ω converter balun. The lighter grey line represents the conductor plane, whereas the darker grey line represents the ground plane. Balun design parameters are given in Table 2. The reflection coefficient and transmission coefficient graphs of the balun as the function of frequency are given in Figure 3 (a) and (b), respectively. Up to 1.5 dB insertion loss is observed within the operating band of the spiral antenna.

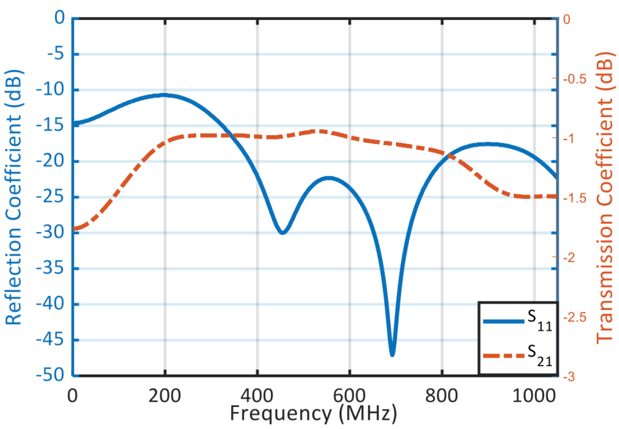

Figure 3. Reflection and transmission coefficients of the balun.

Fractal-Based Ground Plane

The majority of spiral antenna designs use cavity-backed components to ensure unidirectional radiation. The cavity-backed structure of the spiral antenna increases its size, weight, and price. To reduce the dimensions of low-cost, cavity-backed spiral antennas while increasing their gain and axial ratio, it is crucial to develop state of art techniques. Therefore, a fractal reflector surface with a hexagonal cavity is proposed. Figure 4 depicts the geometry of the reflective surface. The structure of the hexagonal fractal consists of three iterations. k = 11.14 mm was used to determine the edge length of the hexagonal unit element. By translating the hexagonal unit element by the wall thickness and rotating it by 60 degrees, additional iterations were generated.

The CST Microwave Studio program was used to analyze the current distributions on the reflecting surface [19]. For TE and TM mode analysis, a plane wave was applied to the structure. Figure 5 depicts the distribution of the surface current on the fractal plane in TE and TM modes.

As seen in the current distributions, capacitive effect exists between the edges of hexagonal unit element. Metallic

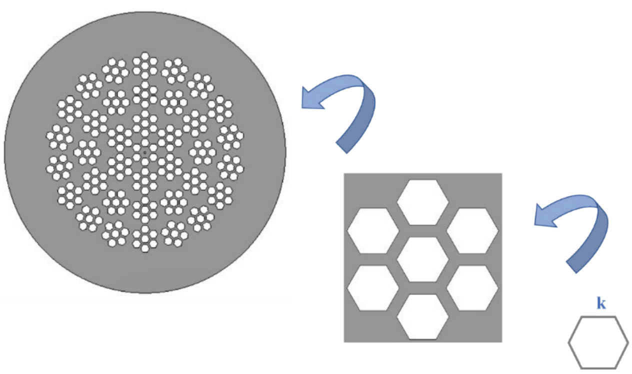

Figure 4. Geometry of hexagonal fractal reflector surface.

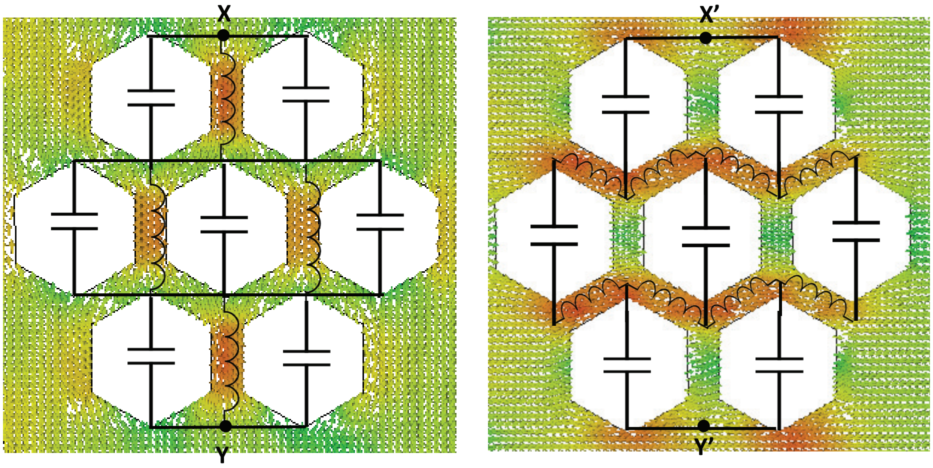

(a) (b)

Figure 5. Current distributions on the surface of the fractal reflector structure (a) TM Mode, (b) TE mode.

surfaces between the hexagonal unit elements exhibit an inductive effect. For the circuits formed by the current distribution, an equivalent circuit solution was developed. For this purpose, series and parallel impedance calculation formula given in Eq. (9-10) were utilized.

$$Z_{Eq} = Z_C + Z_L + \ldots\ldots + Z_N \tag{9}$$

$$\frac{1}{ZEq} = \frac{1}{ZC} + \frac{1}{ZL} + \cdots \frac{1}{ZN} \tag{10}$$

Figure 5 (a) depicts an analysis of the TM mode circuit using the nodal circuit theorem. The circuit is reconfigured according to Figure 6 (a). The nodes are designated with the letters X-C-D-Y, and the circuit is solved.

Using the theory of even-odd circuit analysis, the TE mode circuit shown in Figure 5 (b) was analyzed. For this analysis method's solution, the circuit was reconfigured as depicted in Figure 6 (b). As a consequence of the operations, the $Z_{X'Y'}$ equivalent impedance value is determined. Z_C and Z_L in these equations can be approximately calculated by $Z_C = (16{,}402 * 10^{-12} * k)$ and $Z_L = (1{,}5369 * 10^{-6} * k)$, respectively, where k is a value for the edge length of the hexagonal unit structure [16]. Considering the fractal surface as a load, air region is between the antenna and the surface. Consequently, the TM and TE reflection coefficients are given by Eq. (11-12).

$$\Gamma_{TM} = (Z_{XY} - Z_0)/(Z_{XY} + Z_0) \tag{11}$$

$$\Gamma_{TE} = (Z_{X'Y'} - Z_0)/(Z_{X'Y'} + Z_0) \tag{12}$$

where Z_0 is the free space impedance. The fractal reflective surface structure enhances the circularly polarized radiation and gain of the antenna. Radiation with circular polarization has an axial ratio (AR) of less than 3 dB. The left-to-right axial ratio is represented by

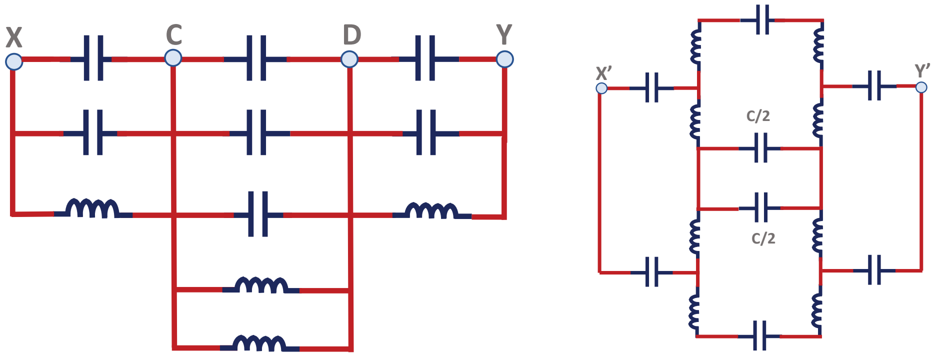

(a) (b)

Figure 6. Equivalent circuits of the (a) TM mode, (b) TE mode.

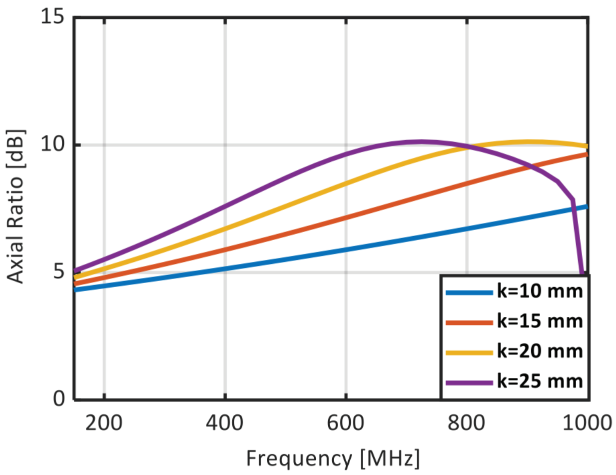

Figure 7. Axial ratio variation of the fractal surface as the function of frequency for different k parameters.

$$LRR = (E_{Left})/(E_{Right}) \tag{13}$$

where E_{Left} and E_{Right} represents the left and right component of the electric field, respectively. The value of the axial ratio (AR) regarding the left and right electric field components is represented as

$$AR = (|1 + |LRR||)/(|1 - |LRR||) \tag{14}$$

To determine the electric fields, the scattering parameters are analyzed by following the procedure given in [16]. The logarithmic expression of the axial ratio value in terms of scattering parameters is obtained by Eq.(15).

$$AR = 20\log\left(\frac{|S_{11}^{RR}|+|S_{11}^{LR}|}{|S_{11}^{RR}|-|S_{11}^{LR}|}\right) = 20\log\left(\frac{|S_{11}^{LL}|+|S_{11}^{RL}|}{|S_{11}^{LL}|-|S_{11}^{RL}|}\right) \tag{15}$$

where s_{11}^{RL} and s_{11}^{LR} are the parameters that defines cross-polarization. S_{11}^{RR} and S_{11}^{LL} are the expressions of co-polarization. To enhance circular polarization, it is necessary to minimize cross-polarization and maximize co-polarization. This is achieved with the designed fractal structure and the axial ratio value, which is an indicator of circular radiation, is improved. The abovementioned procedure is implemented and the variation of the axial ratio as the function of the k parameter of the hexagonal unit element is obtained as given in Figure 7. As k increases, the axial ratio tends to decrease towards higher frequencies. The axial ratio has better results for lower values of k. However, this poses difficulty in the fabrication procedure. After an optimization process in CST, the optimal value of the k parameter of the fractal ground surface is determined as $k = 11.4$ mm

RESULTS AND DISCUSSION

Fabrication

The spiral antenna is constructed by the integration of fractal ground plane, spiral PCB and balun circuit. The spiral and balun are printed on an FR-4 dielectric material with a relative electrical permittivity of $\varepsilon_r = 4.3$ ($tan\delta = 0.018$ @ $1GHz$) and thickness of 1.6 mm. Due to the large diameter of the spiral that makes it possible it operate at 150 MHz (71 cm), the spiral is divided into four quarters and each quarter of the PCB is fabricated separately by chemical etching technique. Then, they are combined from the notches and soldered by their conductors. The hexagonal fractal reflector surface is constructed with an aluminum material having 1mm thickness. Computer Numerical Control (CNC) machining is used for the fabrication. The bulkhead connector of the balun is screwed to the hole at the center of the fractal surface. The differential end of the balun is soldered to the two arms of the spiral conductor. Between the spiral antenna and the fractal reflective surface, polyamide screws with 10 mm diameter are used. Nuts and

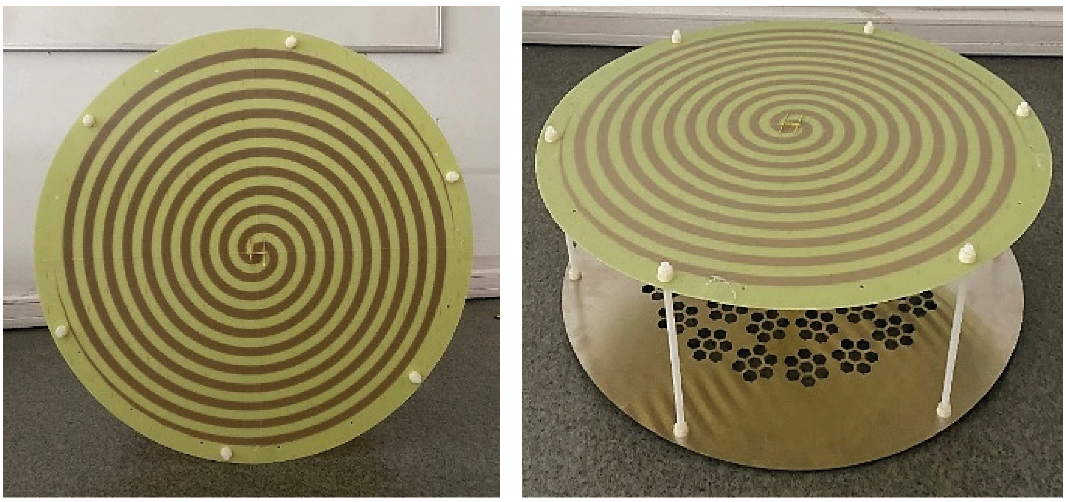

Figure 8. Fabricated spiral antenna with hexagonal fractal reflector surface.

washers are used to fix 27 cm distance between the fractal surface and spiral PCB by the polyamide screws. Figure 8 demonstrates the integrated spiral antenna system with hexagonal fractal reflector surface.

Measurement Results

The refletion coefficient, axial ratio, gain and radiation patterns of the spiral antenna with hexagonal fractal reflector surface is measured with free space measurement technique. Simulation results obtained by CST Microwave Studio, which is a full-wave analysis tool based on finite-integration technique, are also presented. The reflection coefficient variation of the antenna is given in Figure 9 as the fuction of frequency. Acceptable impedance matching is obtained in the whole frequency band of 150-2000 MHz

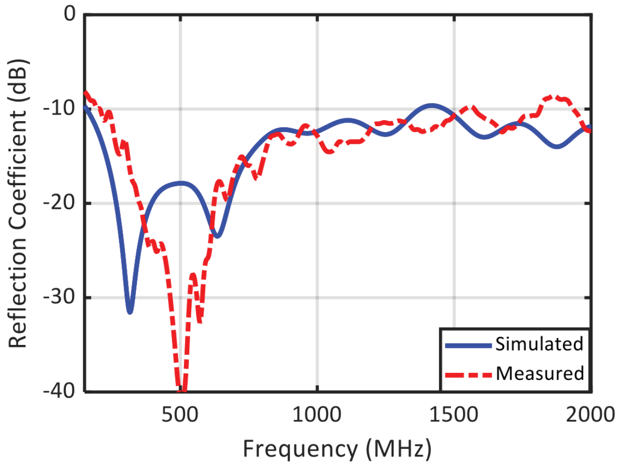

Figure 9. Reflection coefficient variation of the spiral antenna as the function of frequency.

in both simulation and measurement results. The simulation and measurement results show similar characteristics. This figure illustrates very wide band impedance matching characteristic of the spiral antenna, which is 1: 13.3. The simulated and measured axial ratio variation of the spiral antenna is given in Figure 10. Simulation and measurement results indicate that the axial ratio of the antenna is less than 3 dB within the frequency range of 150 MHz to 1050 MHz, with the exception between 190-200 MHz. It is believed that the measurement environment and measurement instruments contribute to the unexpected peaks in the measurement results.

The antenna patterns of the spiral antenna with hexagonal fractal reflector surface are unidirectional due to the fractal reflector surface. The frequency-dependent variation of the antenna gain is given in Figure 11. Although the gain characteristics of the simulation and measurement results show similarity, measured gain variation has a dip between 550-610 MHz. A similar decrease is observed at twice this frequency range. Gain decrease at these frequencies is considered as a resonance effect due to cavity structure. Based on the results of the measurements, the antenna gain is greater than 5 dBi in the frequency range of 140-930 MHz, excluding the band at 490-630 MHz. At 735 MHz, the antenna gain reaches about 10 dBi. The simulated three-dimensional gain patterns of the spiral antenna with fractal reflector surface are given at 160, 300 and 660 MHz in Figure 12. The pattern has realized gain of -6.81 dBi at 160 MHz. The realized gain is 7.8 dBi at 300 MHz, whereas it is 8.96 dBi at 660 MHz. Efficiencies of the antenna are −4.36 dB, −0.93 dB, and −1.76 dB at 160, 300 and 660 MHz, respectively. The measured normalized radiation patterns at 160 MHz, 300 MHz and 650 MHz are given in Figure 13. Measured copolarized patterns in cartesian coordinates shows clear similarity with the three-dimensional simulated patterns given in Figure 12.

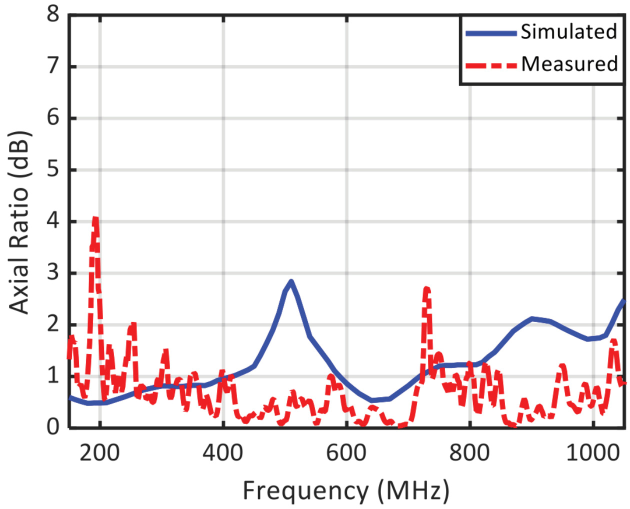

Figure 10. Axial ratio variation of the spiral antenna as the function of the frequency.

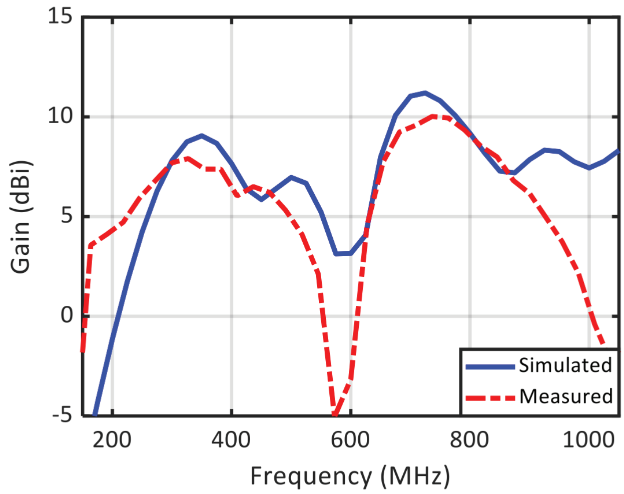

Figure 11. Gain variation of the spiral antenna as the function of the frequency.

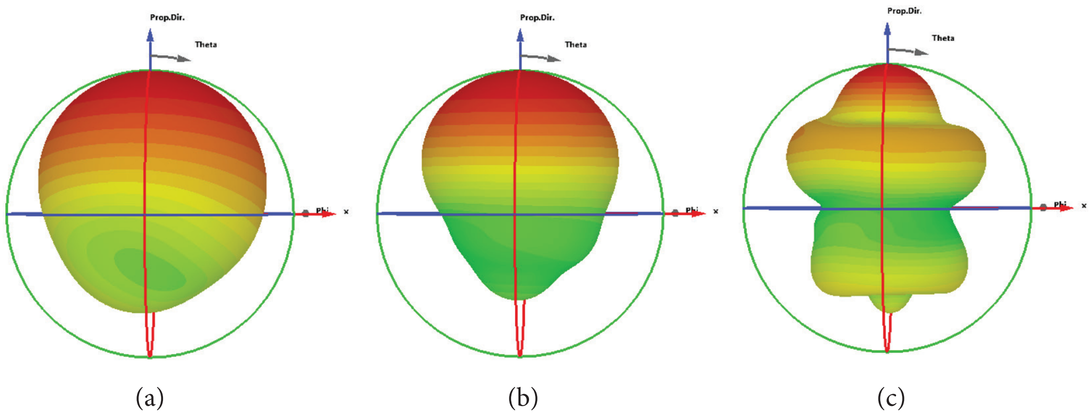

Figure 12. Three-dimensional gain patterns of the spiral antenna at (a) 160 MHz, (b) 300 MHz, (c) 660 MHz.

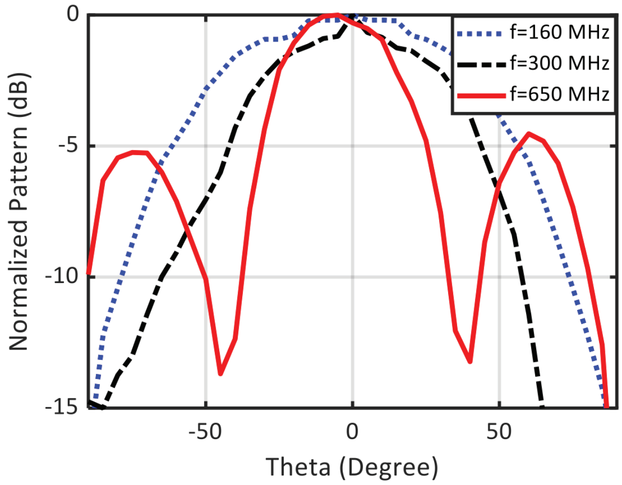

Figure 13. Normalized measured radiation pattern of the spiral antenna at 160, 300 MHz and 660 MHz.

CONCLUSION

A spiral antenna has been designed to satisfy the requirements of high data rate, broadband and broad coverage area, which are essential in numerous fields of wireless communication systems, including satellite systems, military applications, telemetry systems and radars. To enhance the gain and improve the axial ratio, a hexagonal fractal-based reflector surface is added to the spiral antenna. The analysis of fractal surfaces is provided. As one of the size reduction techniques, the tapered arm technique has been utilized and 21.32% size reduction in antenna physical area is obtained. The antenna is fabricated and measured by free space technique. The operating impedance bandwidth of 1:13.3 and 3-dB AR bandwidth of 1:7 is observed in the measurements of the spiral antenna. Due to the fractal reflector, up to 10 dBi measured gain is achieved.

ACKNOWLEDGEMENTS

This work was supported by The Scientific and Technological Research Council of Turkey (Project Number: 121E409). The authors thank TUBITAK for their support.

AUTHORSHIP CONTRIBUTIONS

Authors equally contributed to this work.

DATA AVAILABILITY STATEMENT

The authors confirm that the data that supports the findings of this study are available within the article. Raw data that support the finding of this study are available from the corresponding author, upon reasonable request.

CONFLICT OF INTEREST

The author declared no potential conflicts of interest with respect to the research, authorship, and/or publication of this article.

ETHICS

There are no ethical issues with the publication of this manuscript.

REFERENCES

[1] Kaiser JA. The Archimedean two-wire spiral antenna. IRE Trans Antennas Propag 1960;8:312–323. [CrossRef]

[2] Ely J, Christodoulou C, Shively D. Square spiral microstrip antenna for wireless applications. In: IEEE NTC '95, Microwave Systems Conference Proceedings, 1995.

[3] Hamied FM, El-Rabaie NM, El-Bakry HM, Alshebeili SA. Design and analysis of rectangular spiral nano-antenna for solar energy harvesting. Prog Electromagn Res C 2021;111:25–34. [CrossRef]

[4] Patel NH. Design & implementation of Archimedean spiral antenna with FR4_epoxy sheet. Int J Ind Electron Electr Eng 2020;8:10–13.
[5] Ooi NI, Mohamad SY, Islam MR, Hasbullah NF. Performance comparison between Archimedean and equiangular spiral antenna. J Telecommun Electron Comput Eng 2017;9:105–109.
[6] Baard C, Liu Y, Nikolova N. Ultra-wideband low-cost high-efficiency cavity-backed compound spiral antenna. Electronics 2020;9:1399. [CrossRef]
[7] Zhong YW, Yang GM, Mo JY, Zheng LR. Compact circularly polarized Archimedean spiral antenna for ultra-wideband communication applications. IEEE Antennas Wirel Propag Lett 2016;16:129–132. [CrossRef]
[8] Yoo S, Byun G, Lee C, Choo H. Design of spiral antenna using a Vivaldi-shaped balun. 2019;39:217–226. [CrossRef]
[9] Akkaya E, Gunes F. Ultrawideband, high performance, cavity-backed Archimedean spiral antenna with Phelan balun for direction finding and radar warning receiver applications. Int J RF Microw Comput Aided Eng 2021;31. [CrossRef]
[10] Lee H, Tentzeris MM, Geiger J. Flexible spiral antenna with microstrip tapered infinite balun for wearable applications. In: 2012 IEEE Int Symp Antennas Propag. 2012 [CrossRef]
[11] Liu Q, Ruan CL, Peng L, Wu WX. A novel compact Archimedean spiral antenna with gap-loading. Prog Electromagn Res Lett 2008;3:169–177. [CrossRef]
[12] Ming J, Lizhong S. Design and experimental research on a miniaturized Archimedean spiral antenna. Appl Mech Mater 2012;1618-1621:229–231. [CrossRef]
[13] Park CJ, Yoon YJ. Miniaturization of Archimedean spiral antenna for wideband beamforming arrays. Microw Opt Technol Lett 2019;61:125–130. [CrossRef]
[14] Fu W, Lopez ER, Rowe WST, Ghorbani K. A planar dual arm equiangular spiral antenna. IEEE Trans Antennas Propag 2010;58:1775–1779. [CrossRef]
[15] Yang G, Ye S, Ji Y, Zhang X, Fang G. Miniaturized triple-section spiral antenna with improved radiation. Prog Electromagn Res Lett 2020;94:67–73. [CrossRef]
[16] Ranjbaran SMH, Mohanna S. Improved spiral antenna with a new semi-fractal reflector for short-range sensing. IET Microw Antennas Propag 2018;12:1839–1845. [CrossRef]
[17] Volakis JL. Spiral antennas. In: Antenna Engineering Handbook. 5th ed. New York: McGraw-Hill Education; 2019. p. 18.
[18] Schwinger J, DeRaad LL Jr, Milton K, Tsai W. Babinet's principle. In: Classical Electrodynamics. 2nd ed. Boca Raton (FL): CRC Press; 2024. p. 49.
[19] CST Microwave Studio. CST GmbH, Darmstadt, Germany. Available from: http://www.cst.com Accessed Apr 30 2025.